

A Helicity-Based Method to Infer the CME Magnetic Field Magnitude in Sun and Geospace: Generalization and Extension to Sun-Like/M-Dwarf Stars and Implications for Exoplanet Habitability

S. Patsourakos¹ · M.K. Georgoulis²

© Springer ●●●

Abstract In Patsourakos *et al.* (*Astrophys. J.* **817**, 14, 2016) and Patsourakos and Georgoulis (*Astron. Astrophys.* **595**, A121, 2016) we have introduced a method to infer the axial magnetic field in flux-rope coronal mass ejections (CMEs) in the solar corona and further away in the interplanetary medium. The method, based on the conservation principle for magnetic helicity, uses as input estimates the relative magnetic helicity of the solar source region, along with the radius and length of the corresponding CME flux rope. The method was initially applied to cylindrical force-free flux ropes, with encouraging results. We hereby extend our framework along two distinct lines. First, we generalize our formalism to several possible flux-rope configurations (linear/nonlinear force-free, non force-free, spheromak, torus), to investigate the dependence of the resulting CME axial magnetic field on input parameters and the employed flux-rope configuration. Second, we generalize our framework to both Sun-like and active M-dwarf stars hosting superflares. In a qualitative sense, we find that Earth may not experience severe, atmosphere-eroding, magnetospheric compression even for eruptive solar superflares with energies $\approx 10^4$ times higher than those of the largest *Geostationary Operational Environmental Satellite* (GOES) X-class flares currently observed. In addition, the two recently discovered exoplanets with the highest Earth similarity index, Kepler 438b and Proxima b, seem to lay in the prohibitive zone of atmospheric erosion due to interplanetary CMEs (ICMEs), except in case they possess planetary magnetic fields that are much higher than Earth's.

¹ Section of Astrogeophysics, Department of Physics,
University of Ioannina, 45110 Ioannina, Greece,
spatsour@cc.uoi.gr

² Research Center for Astronomy and Applied Mathematics,
Academy of Athens, Athens, Greece,
manolis.georgoulis@academyofathens.gr

1. Introduction

Knowledge of the magnetic field of coronal mass ejections (CMEs), both near the Sun, and further away at 1 AU, is a key parameter toward understanding their structure, evolution, energetics, and geoeffectiveness. For example, the energy stored in non-potential CME magnetic fields is more than sufficient to counterbalance their mechanical energy (*e.g.* Forbes, 2000; Vourlidas *et al.*, 2000). In addition, the magnitude of the southward interplanetary (IP) magnetic field associated with CMEs reaching 1 AU is arguably the most important parameter for determining the magnitude of the associated geomagnetic storms (*e.g.* Wu and Lepping, 2005). In stellar observations, the recent detections of superflares with energies of up to 10^4 times the energy of “typical” solar flares, on Sun-like stars (*e.g.* Maehara *et al.*, 2012; Shibayama *et al.*, 2013), and their possible association with stellar CMEs, may have significant implications for the physical conditions and the eventual habitability of exoplanets orbiting super-flaring stars (*e.g.* Khodachenko *et al.*, 2007; Lammer *et al.*, 2007; Vidotto *et al.*, 2013; Armstrong *et al.*, 2016; Kay, Opher, and Kornbleuth, 2016). The stellar CME magnetic field at exoplanet orbit is an important parameter for its habitability since it enters into the calculation of the exoplanet magnetosphere size.

Unfortunately, few direct determinations of near-Sun CME magnetic fields currently exist, not to mention stellar CMEs, (*e.g.* Bastian *et al.*, 2001; Jensen and Russell, 2008; Tun and Vourlidas, 2013; Hariharan *et al.*, 2016; Howard *et al.*, 2016; Kooi *et al.*, 2016). These determinations occur from non-routine, exceptional observations in the radio domain (*e.g.* Faraday rotation, moving type IV bursts).

In parallel, methods for CME magnetic field inference have emerged (Kunkel and Chen, 2010; Savani *et al.*, 2015). We have recently developed a novel method to infer the near-Sun and 1 AU magnetic field magnitude. For the remainder of this article, and for brevity, by CME magnetic field we will mean CME magnetic field magnitude. (Patsourakos *et al.*, 2016; Patsourakos and Georgoulis, 2016). In a nutshell, our method is based on the principle of magnetic helicity conservation applied to CMEs. It uses analytical relationships connecting the CME magnetic field with its magnetic helicity H_m , and a set of its geometrical parameters (*e.g.* CME length, radius). Magnetic helicity is a signed quantity, depending on its handedness. For the remainder of this article, and for brevity, when referring to magnetic helicity we will refer to its magnitude.

CME magnetic helicity and geometrical parameters can be routinely deduced from photospheric and coronal observations, respectively. Invoking the magnetic helicity conservation property (*e.g.* Berger, 1984), therefore, allows to infer the CME near-Sun magnetic field. Finally, radial power-law extrapolation of the **inferred** near-Sun CME magnetic field allows to calculate its value at 1 AU. We applied our method to an observed case-study in Patsourakos *et al.* (2016), corresponding to a super-fast CME which gave rise to one of the most intense geomagnetic storms of Solar Cycle 24. In Patsourakos and Georgoulis (2016) we performed a parametric study of our method, based on the observed distributions of its input parameters (CME magnetic helicity and geometrical parameters). We used one of the most common flux-rope CME models (Lundquist 1950).

In the present study we extend our initial work in two meaningful ways: first, we generalize our parametric study on an array of proposed theoretical CME models, thereby further constraining the radial field evolution of the modeled CMEs in the interplanetary medium (Sections 2 and 3). Second, we extend our framework to non-solar cases, particularly to stars hosting superflares, and determine the magnetic fields of possible stellar CMEs associated with these extreme events. This allows us to infer some rough limits on magnetosphere size of exoplanets orbiting such stars and to cast some preliminary implications for their habitability (Section 4). We conclude with a summary and a discussion of our results, as well as possible avenues for future research (Section 5).

2. The Helicity-Based Method to Infer the Near-Sun and 1 AU CME Magnetic Field

We briefly describe here our framework for inferring the near-Sun and 1 AU magnetic field of CMEs, in Sections 2.1 and 2.2, respectively, and its parametrization, in Section 2.3. More details can be found in Patsourakos *et al.* (2016) and Patsourakos and Georgoulis (2016).

2.1. Determination of CME Near-Sun Magnetic Field

First, we infer the near-Sun CME magnetic field as follows:

- i) Determine the magnetic helicity H_m of the CME solar source region using various methods based on theory and photospheric observations (Pariat *et al.*, 2006; Régnier and Canfield, 2006; Georgoulis, Tziotziou, and Raouafi, 2012; Valori, Démoulin, and Pariat, 2012; Moraitis *et al.*, 2014, among others).
- ii) Attribute the source-region H_m to the analyzed CME.
- iii) Determine a set of CME geometrical parameters (*e.g.* radius R , length L) from forward-modeling geometrical fits of multi-view coronal observations of the analyzed CME (Section A of Appendix). Such observations are achieved by coronagraphs typically covering the outer corona.
- iv) Plug the magnetic and geometrical parameters of the CME deduced in the previous two steps into theoretical formulations, such as the models described in Sections B-G of Appendix, and deduce the corresponding near-Sun magnetic field B_* at heliocentric distance r_* .

2.2. Extrapolation of Near-Sun CME Magnetic Field to 1 AU

Next, we extrapolate B_* from r_* , where coronagraphic observations of the CME geometrical properties are taken, outward in the IP space and eventually to 1 AU. We assume that its radial evolution is described by a power-law in the heliocentric radial distance r :

$$B_0(r) = B_*(r/r_*)^{\alpha_B}. \quad (1)$$

In Equation (1) we assume that the power-law index α_B varies in the range $[-2.7, -1.0]$. This results from various theoretical and observational studies (*e.g.*

Patzold *et al.*, 1987; Kumar and Rust, 1996; Bothmer and Schwenn, 1998; Vršnak, Magdalenić, and Zlobec, 2004; Liu, Richardson, and Belcher, 2005; Forsyth *et al.*, 2006; Leitner *et al.*, 2007; Démoulin and Dasso, 2009; Möstl *et al.*, 2012; Poomvises *et al.*, 2012; Mancuso and Garzelli, 2013; Good *et al.*, 2015; Winslow *et al.*, 2015). Notice here that most of these studies do not fully cover the range we are considering here, but typically subsets thereof, either near-Sun or inner heliospheric. We considered 18 equidistant α_B -values and a step of 0.1. In Patsourakos *et al.* (2016) we applied our method to an observed super-fast CME which gave rise to one of the most intense geomagnetic storms of Solar Cycle 24. We found that a rather steep CME magnetic field evolution of the inferred near-Sun CME magnetic field in the IP space, with an index $\alpha_B \simeq -2$, was consistent with the range of the associated interplanetary CME (ICME) magnetic field values as observed in-situ at ≈ 1 AU (*i.e.* at the L1 Lagrangian libration point).

2.3. Parametric Study of the Helicity-Based Method

In Patsourakos and Georgoulis (2016) we performed a parametric study of our method. We carried out Monte-Carlo simulations of 10^4 synthetic CMEs and used the frequently-used Lundquist model (Section B of Appendix). Our simulations randomly sampled 10^4 values of active region (AR) H_m , CME aspect ratio k and angular half-width w from the observed distributions of 42 ARs (Tziotziou, Georgoulis, and Raouafi, 2012) and 65 CMEs (Thernisien, Vourlidas, and Howard, 2009; Bosman *et al.*, 2012), respectively. Using the randomly selected CME aspect ratio and angular half-width in Equations (4) and (5), the CME radius and length, respectively, were deduced, and finally, the CME magnetic field was determined via Equations (6) and (7). As a result, 10^4 B_* values at $r_* = 10 R_\odot$ were calculated. These near-Sun magnetic fields were then extrapolated to 1 AU, therefore leading to 180,000 1 AU CME magnetic field values, resulting from the matrix of 10^4 B_* and 18 α_B values discussed in Sections 2.1 and 2.2. We found that an index $\alpha_B = -1.6 \pm 0.2$ led to a ballpark, statistical agreement between the model-predicted ICME magnetic field distributions and actual ICME observations at 1 AU.

3. Parametric Study of the Helicity-Based Method for Different CME Models

In this Section we extend and generalize the parametric study of Patsourakos and Georgoulis (2016) to six different CME models, including the Lundquist model used in that study. These models, described in Sections B-G of Appendix, make different assumptions about the CME shape (cylindrical segment, toroidal, spheromac), the nature of their currents (linear/nonlinear force-free, non force-free) and the distribution of twist (uniform, non-uniform), thereby allowing maximum flexibility in our method's application.

As in Patsourakos and Georgoulis (2016), we perform Monte-Carlo simulations picking up 10^4 random deviates from the observed distributions of the

input magnetic (H_m) and geometrical (k and w) parameters of our method and determine $10^4 B_*$ values for each considered model using the corresponding equations per model (Sections B-G of Appendix). Depending on the specific model assumptions, extra geometrical parameters are used (*e.g.* CME minor and major radius in Equation (9); number of turns in Equations (11) and (13)). For each considered model we calculate the probability density function (PDF) of: (1) the extrapolated to 1 AU CME magnetic fields, $wB_{1 \text{ AU}}$, for the $10^4 B_*$ values and for each of the 18 considered α_B values, PDF_{mod} ; and (2) the magnetic fields, B_{MC} , for 162 magnetic clouds (MCs) observed at 1 AU as resulting from their linear force-free fits (Lynch *et al.*, 2003; Lepping *et al.*, 2006), and PDF_{obs} .

We compare the results of our Monte-Carlo simulations for the six different employed models with MC observations in Figures 1 and 2. In Figure 1 we display the correlation coefficient of PDF_{mod} and PDF_{obs} as a function of α_B , whereas in Figure 2 we display the fraction frac_{MC} of $B_{1 \text{ AU}}$ values falling within the observed B_{MC} range, namely [4,45] nT, as a function of α_B .

Several remarks can be now made:

- i) Both PDF_{mod} versus PDF_{obs} correlation coefficients and frac_{MC} exhibit well-defined peaks, and cover similar α_B -ranges of $\approx [-1.85, -1.2]$ and $[-2.0, -1.3]$, respectively, for all considered models. For the cases of the toroidal and spheromak linear force-free models there are secondary peaks for $\alpha_B < -2$ (Figure 1). However these peaks are not supported by high frac_{MC} -values.
- ii) Similar (relatively high) peak values can be found in both Figures 1 (≈ 0.9) and 2 (≈ 0.7) for all considered models. The full width at half maximum (FWHM) of the curves of Figures 1 and 2 is $\approx [0.3, 0.5]$ and $[0.7, 0.8]$, respectively, in the α_B -range.
- iii) The linear and nonlinear force-free, cylindrical, flux-rope models, black and red lines, respectively, in both Figures 1 and 2, place the median of the considered models.

Figure 3 displays the model-averaged PDF_{mod} versus PDF_{obs} correlation coefficient and frac_{MC} as a function of α_B . These plots encapsulate the overall performance of all considered models. The corresponding curves peak at $\alpha_B \approx -1.6$ and $\alpha_B \approx -1.8$ for the PDF_{mod} versus PDF_{obs} correlation coefficient and frac_{MC} , respectively. Both peaks correspond to relatively high values of ≈ 0.6 .

4. Extension to Stellar CMEs

Existing stellar observations lack the spatial resolution to directly image possible stellar CMEs, not to mention their source regions. Therefore, we have to rely on indirect observational inferences for stellar CMEs (*e.g.* Houdebine, Foing, and Rodono, 1990; Leitzinger *et al.*, 2011; Osten *et al.*, 2013; Leitzinger *et al.*, 2014). Solar observations suggest that with increasing flare magnitude, the probability of an associated CME is also increasing, with GOES-class flares $\gtrsim X3$ essentially associated one-to-one to fast or superfast CMEs (*e.g.* Andrews, 2003; Yashiro *et al.*, 2005; Nindos *et al.*, 2015; Harra *et al.*, 2016). Therefore, it is possible that

stars with superflares could have enhanced rates of superfast CMEs associated to them. Stars hosting superflares are generally characterized by enhanced magnetic activity, as inferred from their larger chromospheric emissions (*e.g.* Karoff *et al.*, 2016). A common practice in studies of stellar flares and CMEs is to extrapolate empirical relationships derived from solar studies to the stellar context (*e.g.* Aarnio, Matt, and Stassun, 2012; Drake *et al.*, 2013; Osten and Wolk, 2015).

Therefore, in order to determine the H_m associated with stellar CMEs, we rely on a recently discovered empirical relationship connecting the free coronal magnetic energy E_f and H_m of solar active regions. Tziotziou, Georgoulis, and Raouafi (2012) inferred the following best fit for 42 solar ARs and 162 snapshots thereof:

$$\log|H_m| = 53.4 - 0.0524(\log(E_f))^{0.653} \exp\left(\frac{97.45}{\log(E_f)}\right). \quad (2)$$

Equation (2) was applied to an E_f interval of $10^{30} - 10^{33}$ erg. We consider stellar eruptive flares (*i.e.* associated with stellar CMEs) with energies in the range $10^{32} - 10^{36}$ erg, and cover this interval with a logarithmic step of 0.1 leading to $41(=N_{E_f})$ bins in E_f . The employed interval includes both solar flares and stellar superflares (*e.g.* Shibayama *et al.*, 2013); stellar superflares have a most probable energy of few times 10^{34} erg. Notice that typically the quoted superflare energies are bolometric, *i.e.* correspond to the wavelength-integrated radiated energy (*e.g.* Maehara *et al.*, 2012; Shibayama *et al.*, 2013). For each considered flare energy we assume an equal free magnetic energy. This assumption imposes a lower limit on the free magnetic energy of the host active region, since we know that the largest flare in an active region releases a relatively small percentage (typically 10–20%) of the free magnetic energy stored in the region (*e.g.* Lynch *et al.*, 2008; Sun *et al.*, 2012; Tziotziou, Georgoulis, and Raouafi, 2012; Tziotziou, Georgoulis, and Liu, 2013).

Having determined the magnetic helicities that could be associated with stellar CMEs, we then adopt typical values for k ($=0.3$) and w ($=20$ degrees) as resulting from solar studies of CMEs (*e.g.* Thernisien, Vourlidas, and Howard, 2009; Bosman *et al.*, 2012) and determine their near-star stellar CME magnetic field values at $10 R_\odot$ by applying the Lundquist model (Section B of Appendix). Next, adopting the radial power-law CME magnetic field evolution of Equation (1), we extrapolate the derived near-star stellar CME magnetic fields in the range $[0.05, 1.5]$ AU, which spans the habitable zone (HZ) of exoplanet candidates (Kane *et al.*, 2016). HZ is typically defined as the distance from a mother star at which water could exist in a liquid form (*e.g.* Kasting, Whitmire, and Reynolds, 1993; Selsis *et al.*, 2007; Khodachenko *et al.*, 2007). This obviously corresponds to a minimum requirement for life-sustaining conditions in exoplanets. The HZ migrates closer to the mother star when moving from Sun-like stars to M-dwarfs (*e.g.* see Figure 3 in Selsis *et al.*, 2007).

We cover the above-mentioned radial distance interval with a radial step of 0.003 AU, leading to $480(=N_r)$ bins in radial distance. We assume that this interval is populated with exoplanets having a magnetosphere. For the extrapolation we employ an index $\alpha_B = -1.6$ since it corresponds to the “best-fit” for the Lundquist model for the solar-terrestrial case (Patsourakos and Georgoulis,

2016). We therefore calculate a two-dimensional, $41 \times 480 N_{\text{r}}$ versus $N_{E_{\text{f}}}$ grid of extrapolated stellar CME magnetic fields, at the locations of hypothetical exoplanets and for the employed stellar flare energies. We finally determine the magnetopause radius of hypothetical exoplanets at the considered distance from a pressure-balance equation, balancing the stellar CME magnetic pressure at the exoplanet’s vicinity with the magnetic pressure of the intrinsic, assumed dipolar, planetary magnetic field (*e.g.* Chapman and Ferraro, 1930):

$$\frac{B_{\text{CME}}^2}{8\pi} = \frac{B_{\text{eq}}^2}{8\pi} \left(\frac{1}{r_{\text{mpause}}} \right)^6. \quad (3)$$

In Equation (3), B_{CME} is the extrapolated stellar CME magnetic field at the vicinity of the exoplanet, B_{eq} is the planetary equatorial magnetic field, and r_{mpause} is the magnetopause radius, assumed a dimensionless number in planetary radius (R_{p}) units. In writing Equation (3) we assume a spherical magnetosphere. Given CMEs are magnetically-dominated structures, neglecting their thermal and ram pressure in Equation (3) can be justified.

In Figure 4 we depict a color representation of the exoplanet magnetopause radius as a function of exoplanet distance and stellar flare magnitude. Given that current knowledge of magnetic fields in exoplanets is incomplete, we first assume that B_{eq} is equal to the (current-day) terrestrial equatorial magnetic field ($B_{\text{E}}=0.333$ G). Values of r_{mpause} smaller than $2 R_{\text{p}}$ are saturated with black. This threshold corresponds to the minimum magnetosphere size that could prevent atmospheric erosion from stellar CME impacts (Khodachenko *et al.*, 2007; Lammer *et al.*, 2007; Scalo *et al.*, 2007) and may be viewed as an additional, necessary condition for habitability. The maximum r_{mpause} is $\approx 10R_{\text{p}}$, close to the unperturbed value for the terrestrial magnetosphere. From Figure 4 we notice that for exoplanets at distances $\lesssim 0.1$ AU, practically all considered flare energies lead to magnetospheric compression below the $2 R_{\text{p}}$ “habitability threshold” discussed above. Exoplanets at distances $\gtrsim 0.4$ AU have $r_{\text{mpause}} \gtrsim 2R_{\text{p}}$ for all considered flare energies.

Moreover, exoplanets that are relatively close to their mother star could be subject to tidal locking, *i.e.* synchronization between their rotational and orbital periods, and generally a decrease in their rotation rate (*e.g.* Gladman *et al.*, 1996). Slowing-down of an exoplanet leads to a decrease of its magnetic field (*e.g.* Grießmeier *et al.*, 2004, 2005). In Figures 5 and 6 we calculated r_{mpause} for two more cases, $B_{\text{eq}} = 0.25B_{\text{E}}$ and $B_{\text{eq}} = 0.061B_{\text{E}}$, respectively. These values correspond to calculations of planetary magnetic moments of Earth-like exoplanets in the close vicinity of M-type dwarf stars subject to tidal-locking (Khodachenko *et al.*, 2007). The maximum r_{mpause} is $\approx 6R_{\text{p}}$ and $\approx 4R_{\text{p}}$, for Figure 5 and 6, respectively. Decrease of the exoplanet magnetic field leads to further compression of its magnetopause radius for a given stellar flare energy, with exoplanets at distances $\lesssim 0.2$ and $\lesssim 0.4$ AU, for $0.25 B_{\text{E}}$ and $0.061 B_{\text{E}}$, respectively, with $r_{\text{mpause}} < 2R_{\text{p}}$. In the case corresponding to $0.25 B_{\text{E}}$ (Figure 5) exoplanets at distances $\gtrsim 1$ AU have $r_{\text{mpause}} > 2R_{\text{p}}$ for all considered flare energies. Moreover, in the case corresponding to $0.061 B_{\text{E}}$ (Figure 6), only stellar flares with energies up ten times the lower limit ($= 10^{33}$ erg) of superflares could

result in $r_{\text{mpause}} > 2R_{\text{p}}$ for exoplanets at distances $\gtrsim 0.7$ AU. Exoplanets at 1 AU experience magnetospheric compression below $2R_{\text{p}}$ only in the case of the smallest considered exoplanet magnetic field resulting from tidal locking (Figure 6).

Figures 4–6 include two case-studies of recently detected exoplanets orbiting stars hosting superflares. These are Kepler 438b (Torres *et al.*, 2015; Armstrong *et al.*, 2016) and Proxima b (Anglada-Escudé *et al.*, 2016; Davenport *et al.*, 2016), orbiting M-type dwarfs Kepler 438 and Proxima Centauri, respectively. Kepler 438b (Proxima b) have orbits with semi-major axis of 0.16 (0.04) AU and their mother stars exhibit superflares with energies 1.4×10^{33} (10^{33}) erg. Kepler 438b and Proxima b have the highest Earth Similarity Index (ESI), 0.88 and 0.87, respectively, amongst the detected exoplanets to date¹. The ESI of a given exoplanet is a metric of its degree of resemblance with Earth in terms of mass, radius *etc.* An ESI equal to 1 suggests a perfect match of the exoplanet with Earth. From Figures 4–6 we gather that for all considered stellar flare energies and planetary magnetic fields, the hypothesized stellar CMEs result in severe magnetospheric compression, below $2R_{\text{p}}$ for both Kepler 438b and Proxima b. This appears to be a strong constraint against habitability of these exoplanets.

We finally investigate the effect of CMEs associated with potential solar superflares on the terrestrial magnetosphere. Based on our current understanding of solar dynamo and magnetic fields, geological and historical records, and superflares observed in Sun-like stars one may not exclude the rare (*i.e.* over timescales of several centuries or more) occurrence of relatively small superflares (energies of up to $\approx 10^{34}$) on the Sun (*e.g.* Shibata *et al.*, 2013; Usoskin *et al.*, 2013; Nogami *et al.*, 2014; Toriumi *et al.*, 2017), although such possibility has been contested (*e.g.* Schrijver *et al.*, 2012; Aulanier *et al.*, 2013; Cliver *et al.*, 2014). Inspection of Figure 4, more specifically by considering a vertical cut at a distance equal to 1 AU, shows that solar superflares with energies exceeding 10^{33} and 10^{34} erg could lead to significant compression of the terrestrial magnetosphere at ≈ 6 and 5 Earth radii, respectively, in the case $\alpha_B = -1.6$ (Figure 7). For a steeper index $\alpha_B = -1.9$, the magnetopause distance stays above 6 Earth radii for a superflare with energy 10^{34} erg (Figure 8). Importantly, in no case does the magnetopause distance become smaller than 2 Earth radii, even for a “worst-case” superflare with energy 10^{36} erg.

5. Discussion and Conclusions

5.1. Summary of our Findings and Outlook

In this work, we (a) perform a parametric study of inferring the near-Sun and 1 AU magnetic field of CMEs using an array of analytical CME models, and (b) apply our method to stars hosting superflares. A summary of findings is as follows:

¹See phl.upr.edu/projects/habitable-exoplanets-catalog/data.

- i) All considered CME models lead to predicted CME magnetic fields at 1 AU which largely recover the distribution and fall within the range of magnetic cloud observations at 1 AU, as shown in Figures 1 and 2, respectively.
- ii) The best agreement between the predicted and observed CME magnetic fields at 1 AU is achieved in a different α_B -range for each model. For all considered models this range corresponds to $\alpha_B \in [-2.0, -1.2]$. No model appears to significantly outperform the others in terms of agreement between extrapolated CME fields and observations at L1.
- iii) Stellar CMEs associated with flares and superflares with energies $10^{32} - 10^{36}$ erg could compress the magnetosphere of exoplanets with terrestrial magnetic field orbiting at < 0.1 AU below the magnetopause-distance threshold of 2 planetary radii (Figure 4). This threshold signals a CME-induced atmospheric erosion. This zone of severe compression shifts to < 0.3 AU for flare energies of 10^{34} erg.
- iv) A CME associated with a solar superflare of 10^{34} erg may compress our magnetosphere to a magnetopause distance of ≈ 5 Earth radii (Figure 7), about half of its unperturbed value. Even an extreme superflare of 10^{36} erg cannot push the magnetopause distance to a value lower than 2 Earth radii.
- v) For exoplanets with weaker magnetic fields than Earth, particularly tidally locked ones, a superflare can cause severe magnetospheric compression below the 2 planetary radii limit at astero-centric distances < 0.3 and 0.4 AU (Figures 5 and 6, respectively).
- vi) Severe compressions of potential magnetospheres below 2 planetary radii are obtained for exoplanets Kepler 438b and Proxima b (Figures 4–6). The close distance of these exoplanets to mother stars Kepler 438 and Proxima Centauri, respectively, is the main reason for this rather strict constraint on these exoplanet’s habitability.

Our major conclusion is that all employed CME models, in spite of differences in key properties (distribution of electric currents, geometry *etc.*) perform similarly at 1 AU, if applied following the corresponding “best-fit” α_B ranges. This suggests that, for statistical space-weather forecasting purposes, any of these models can be applied. For a more detailed treatment between models, aiming toward an improved understanding of the CME-ICME transition and physical state, one needs detailed model comparisons on a case-by-case basis at 1 AU (*e.g.* Riley *et al.*, 2004; Al-Haddad *et al.*, 2013). Inner heliospheric and coronal in-situ and imaging observations are also in high demand, hence anticipation is mounting for the upcoming *Solar Orbiter* and *Solar Probe Plus* missions.

A core assumption of the solar-IP part of our analysis is that the entire source-region helicity is attributed to the corresponding CMEs. This overestimates the helicity shed by CMEs, since one can rather reasonably expect that only a fraction of the available H_M is expelled in single CME events. If the entire helicity content of the source active region was shed in a single event, that would mean zero remaining free energy, which would be untenable with the essentially unchanged, line-tied photosphere. Further, there may not be enough time to build-up from zero the helicity expelled in homologous eruptions. CMEs shedding only a fraction of the source-region H_M can also be reached by statistical considerations: for instance, the eruptive AR H_M distributions have most probable

values $> 10^{43} \text{Mx}^2$, (*e.g.* Nindos and Andrews, 2004; Tziotziou, Georgoulis, and Liu, 2013), while the MC ones at 1 AU are about an order of magnitude smaller (*e.g.* Lynch *et al.*, 2005). In addition, analysis of the cumulative H_{M} shed by CMEs over long intervals covering large fractions of (or entire) solar cycles, combined with CME occurrence rates, AR characteristics and MC H_{M} values at 1 AU, leads to the conclusion that on average a CME expels $\approx 10 - 20\%$ of the AR H_{M} (DeVore, 2000; Georgoulis *et al.*, 2009; Démoulin, Janvier, and Dasso, 2016). Next, a handful of case-studies monitored eruption-associated H_{M} changes in the lower solar atmosphere and/or compared the source region H_{M} with the H_{M} of the associated MC at 1 AU, and found that the observed CMEs expel $\approx 10 - 70\%$ of the available H_{M} (*e.g.* Démoulin *et al.*, 2002; Green *et al.*, 2002; Nindos, Zhang, and Zhang, 2003; Luoni *et al.*, 2005; Mandrini *et al.*, 2005; Kazachenko *et al.*, 2009; Nakwacki *et al.*, 2011; Tziotziou, Georgoulis, and Liu, 2013). In practice, however, most of these studies showed that eruption-related H_{M} changes amount to only $\approx 10 - 40\%$ of the available H_{M} , notwithstanding the significant uncertainties due to the various methods and H_{M} determinations. Finally, magnetohydrodynamical (MHD) models of CMEs based on largely different initiation scenarios show that $\approx 10 - 40\%$ of the available H_{M} leaves the corresponding computational boxes with the simulated CMEs (*e.g.* MacNeice *et al.*, 2004; Gibson and Fan, 2008; Kliem, Rust, and Seehafer, 2011; Moraitis *et al.*, 2014).

From the discussion above, and bearing in mind the corresponding uncertainties, it is reasonable to assume that CMEs, on average, shed $\approx 10 - 40\%$ of the source region H_{M} . To investigate this, we repeat the calculations of Sections 2 and 3, using this time CME H_{M} values randomly selected from $10 - 40\%$ of the employed AR H_{M} (step 2 in Section 2.1). In Figure 9, we display the resulting model-averaged $\text{PDF}_{\text{mod}} - \text{PDF}_{\text{obs}}$ correlation coefficient and frac_{MC} as a function of α_B . Comparison of the results of Figure 9 and Figure 3, corresponding to the assumption that the entire AR H_{M} is attributed to the associated CME, shows that the curves of Figure 9 are shifted towards larger (*i.e.* flatter) α_B -values by ≈ 0.3 , for both $\text{PDF}_{\text{mod}} - \text{PDF}_{\text{obs}}$ and frac_{MC} . Requiring flatter α_B -values for smaller H_{M} is reasonably anticipated. This further leads to smaller near-Sun CME magnetic fields, and therefore the CME magnetic field should evolve less abruptly with radial distance to match the MC observations at 1 AU. Besides this displacement, the overall shapes, peak values and widths of the curves reported in Figures 3 and 9 are similar.

Several improvements can be envisioned for both the solar and the stellar part of our study. For example, currently our method does not incorporate CME orientation and rotation in the interplanetary space en route to 1 AU, thereby preventing the calculation of the vector magnetic field in CMEs. Rather straightforward-to-implement recipes to incorporate this element exist (*e.g.* Thernisien, Vourlidas, and Howard, 2009; Wood, Howard, and Socker, 2010; Kay, Opher, and Evans, 2013; Isavnin, Vourlidas, and Kilpua, 2014; Savani *et al.*, 2015). In addition, eruption-related helicity changes as found in Tziotziou, Georgoulis, and Liu (2013), are more appropriate to use on a case-by-case application of our method, as performed in Patsourakos *et al.* (2016). The contribution of magnetic helicity associated with magnetic reconnection of the erupting flux

with its surroundings could be also important (Priest, Longcope, and Janvier, 2016). Better statistics of eruption-related changes are clearly needed.

In the stellar application of our method, a major, largely unconstrained working hypothesis is that the Tziotziou, Georgoulis, and Raouafi (2012) relationship between AR helicity and free-magnetic energy (Equation (2)), derived for solar ARs, can be extended to stellar ARs. This requires further investigation. For example, one may derive some rough estimates of stellar AR helicities by using observations of starspot size and magnetic flux as derived by Zeeman-Doppler imaging techniques (*e.g.* Semel, 1989; Donati *et al.*, 2008; Vidotto *et al.*, 2013). Such estimates could be then linked to worst-case flare-energy scenarios triggered in these stars. Finally, better constraints, both modeling and observational, of exoplanet magnetic fields, are required in order to predict more reliably the influence of stellar CME impacts, and of stellar winds in general, on exoplanet magnetospheres.

5.2. Connection to Previous Studies

Let us now briefly discuss pertinent, complementary efforts to assess the size of exoplanet magnetospheres around M-dwarf and Sun-like stars. Khodachenko *et al.* (2007) found that the ram-pressure of stellar CMEs could significantly compress (altitudes < 1000 km) the magnetosphere of Earth-like exoplanets, subject to tidal locking, at distances < 0.1 AU around active M stars. By extrapolating surface magnetic fields of 15 active dM stars, as derived by Zeeman-Doppler imaging, at locations of exoplanets in their HZ, Vidotto *et al.* (2013) found that Earth-like exoplanets would require stronger intrinsic magnetic fields than the terrestrial case, in order to have a magnetosphere with a radius comparable to that of Earth. Using models and empirical relationships described in See *et al.* (2014) and Vidotto *et al.* (2014), Armstrong *et al.* (2016) found that the extrapolated Kepler 438 to Kepler 438 b stellar wind and magnetic field pressure leads to a magnetospheric radius for Kepler 438b that is similar to the terrestrial one. They, however, assumed that Kepler 438b has a magnetic field equal to the terrestrial case, an assumption which possibly overestimates the magnetopause radius of Kepler 438b, since its semi-major axis is small (≈ 0.16 AU), so it may experience tidal locking and a decrease in its magnetic field.

Extrapolation of surface magnetic fields combined with stellar wind models, and extrapolation of assumed stellar CME magnetic fields, to close-orbit exoplanets around M dwarfs showed that exoplanet fields of a few tens to hundreds of Gauss, significantly higher than the terrestrial one, are required to maintain a magnetopause radius of $2R_p$ (Kay, Opher, and Kornbleuth, 2016). The bulk of these studies, including ours, in spite of different settings and assumptions, essentially reach the same basic conclusion, namely, that exoplanets in the close proximity of their mother stars, could experience significant compression due to stellar wind and CMEs that may further hamper their habitability. An example along these lines in our solar system is the recent finding from the Mars Atmosphere and Volatile Evolution (MAVEN) mission team that ICMEs interacting with the Martian magnetosphere in the early history of the planet may have played an important role in the planet's atmospheric erosion (Jakosky *et al.*,

2015). Here, of course, it is not the planet’s heliocentric distance – which is larger than Earth’s – but its weak magnetic field, that has been the major cause for this development. In a related study, See *et al.* (2014) studied the effect of stellar winds on the sizes of a hypothetical Earth, around 124 Sun-like stars. They found that in most cases, the magnetospheric radius takes values > 5 terrestrial radii. This is probably a lower limit, because the ram and magnetic pressure of stellar CMEs is not taken into account.

Recent work on the astrosphere of Proxima Centauri and the intrinsic magnetic field of Proxima b suggest significant compression of their potential magnetospheres, fully aligned with our results. 3D MHD stellar wind and magnetic field models around Proxima Centauri, show that the total stellar wind pressure at Proxima b, could be 2000 times higher than the corresponding one at Earth (Garraffo, Drake, and Cohen, 2016). In addition, planetary evolution models, scaled to Proxima b, predict a current-day magnetic moment of Proxima b of ≈ 0.32 of the current terrestrial one (Zuluaga and Bustamante, 2016). Finally, recent work by Airapetian *et al.* (2017) and Dong *et al.* (2017), using MHD simulations, demonstrated the realism of very significant atmospheric losses in Proxima b.

Notice here that tidal locking is achieved for Earth-like exoplanets around G-M type stars at distances smaller than $\approx 0.4 - 0.7$ AU (*e.g.* see Figure 2 of Grießmeier *et al.*, 2005). Such calculations include only the effect of gravitational tides. Inclusion of thermal tides linked to the existence of a planetary atmosphere, internal dissipation effects, eccentric orbits *etc.*, could bring exoplanets into asynchronous rotation (*e.g.* Cunha, Correia, and Laskar, 2015; Leconte *et al.*, 2015). However, this applies mostly to exoplanets not very close to their mother stars. Cunha, Correia, and Laskar (2015) found for a set of 90 Earth-sized exoplanets with major semi-axes in the range 0.004-0.54 AU that they are largely synchronized (see their Table 1).

Disclosure of Potential Conflicts of Interest

The authors declare that they have no conflicts of interest.

Acknowledgements

The authors thank the referee for a useful suggestion to investigate the impact of the uncertainty of the erupted helicity. This research has been partly co-financed by the European Union (European Social Fund -ESF) and Greek national funds through the Operational Program “Education and Lifelong Learning” of the National Strategic Reference Framework (NSRF) -Research Funding Program: “Thales. Investing in knowledge society through the European Social Fund”. SP acknowledges support from an FP7 Marie Curie Grant (FP7-PEOPLE-2010-RG/268288). MKG wishes to acknowledge support from the EU’s Seventh Framework Programme under grant agreement no PIRG07-GA-2010-268245. The authors acknowledge the Variability of the Sun and Its Terrestrial Impact (VarSITI) international program.

Appendix

The Appendix presents a short description of a geometrical CME model used in the current investigation (A). Moreover, it contains short descriptions and equations relating magnetic field magnitude with H_m and various geometrical parameters for various theoretical CME models (B–G).

A. Deducing CME Geometrical Parameters from the GCS Model

To obtain the geometrical parameters R and L we adopt the Graduated Cylindrical Shell (GCS) forward fitting model of Thernisien, Vourlidas, and Howard (2009). This is a geometrical flux-rope model routinely used to fit the large-scale appearance of flux-rope CMEs in multi-viewpoint observations acquired by coronagraphs onboard the *Solar and Heliospheric Observatory* (SOHO) and *Solar Terrestrial Relations Observatory* (STEREO) spacecraft. The GCS user modifies a set of free parameters (CME height, half-angular width w , aspect ratio k , tilt angle, central longitude and latitude) to achieve a best-fit agreement between the model and observations. A detailed description can be found in Thernisien, Vourlidas, and Howard (2009).

In the framework of the GCS model, the CME radius R at a heliocentric distance r is given by the following Equation:

$$R(r) = kr. \quad (4)$$

To assess the flux-rope length L , it is assumed that the CME front is a cylindrical section (see Figure 1 of Démoulin and Dasso (2009)) with an angular width provided by the geometrical fitting. One may then write

$$L = 2wr_{\text{mid}}, \quad (5)$$

where r_{mid} is the heliocentric distance half-way through the model's cross section, along its axis of symmetry. The half-angular width w is given in radians.

B. Cylindrical Linear Force-Free Model

The Lundquist flux-rope model (Lundquist, 1950) is arguably the most commonly used flux-rope model and corresponds to a cylindrical force-free solution.

From Dasso *et al.* (2006) we get for a Lundquist flux rope:

$$H_m = \frac{4\pi B_0^2 L}{\alpha} \int_0^R J_1^2(\alpha r) dr, \quad (6)$$

with L and R the flux-rope length and radius, respectively, J_1 the Bessel function of the first kind, B_0 the maximum axial field, and α the force-free parameter.

Making the common assumption of a purely axial (azimuthal) magnetic field at the flux-rope axis (edge) we get:

$$\alpha R = 2.405. \quad (7)$$

C. Cylindrical Nonlinear Force-Free Model

This cylindrical nonlinear force-free flux-rope model was proposed by Gold and Hoyle (1960). From Dasso *et al.* (2006) we have:

$$H_m = L \left(\frac{8\pi [\ln(1 + U^2/4)]^2}{U^2} \right) B_0^2 R^4 \tau_0, \quad (8)$$

with $U = 2\tau_0 R$ and $\tau_0 = \frac{1}{2}\alpha$.

D. Toroidal Linear Force-Free Model

This toroidal force-free model was proposed by Vandas and Romashets (2016):

$$H_m = (2\pi H) \frac{B_0^2 \pi H^3}{4\alpha_0} \left[8 - \left(1 + \frac{1}{\alpha_0^2} \right) \frac{R^2}{H^2} \right] J_1^2(\alpha_0), \quad (9)$$

with $H = r_{\text{mid}}$ and R the torus major and minor axis, respectively, and $\alpha_0 = 2.405$. R and r_{mid} are the same as in Equation (4).

E. Linear Force-Free Model Spheromac

This linear force-free spheromac model was proposed by Kataoka *et al.* (2009):

$$H_m = 0.045 r_{\text{mid}}^4 B_0^2, \quad (10)$$

and corresponds to a Sun-centered sphere with radius r_{mid} meant to approximate a spherical magnetic cloud. The value of r_{mid} is the same as in Equation (4).

F. Cylindrical Constant Current Non Force-Free Model

This cylindrical constant current non-force model was proposed by Hidalgo *et al.* (2000) and generalized by Nieves-Chinchilla *et al.* (2016).

From Dasso *et al.* (2006) we have that:

$$H_m = \frac{7\pi}{30}\tau_0 LR^4 B_0^2, \quad (11)$$

where τ_0 is the twist per unit length at the flux-rope axis. The twist parameter τ_0 can be written as:

$$\tau_0 = \frac{N_{\text{turns}}}{L}, \quad (12)$$

with N_{turns} the total number of field turns along the flux-rope axis. To estimate τ_0 we use L as calculated in Section A of Appendix and assume that N_{turns} is equal to 0.5 and 10, corresponding to the extreme cases between a weakly and a strongly twisted (multi-turn) flux-rope, respectively. The number of N_{turns} covering this interval can be deduced from solar imaging and magnetic field observations (via photospheric magnetic field extrapolations) (*e.g.* Vrsnak *et al.*, 1993; Gary and Moore, 2004; Guo *et al.*, 2013; Chintzoglou, Patsourakos, and Vourlidas, 2015) and MC fits at 1 AU (*e.g.* Hu *et al.*, 2014; Wang *et al.*, 2016).

G. Cylindrical Linear Azimuthal Current Non Force-Free Model

This cylindrical linear azimuthal current non force-free model was proposed by Cid *et al.* (2002) and generalized by Nieves-Chinchilla *et al.* (2016). In this model the azimuthal current increases with distance from the flux-rope axis.

From Dasso *et al.* (2006) we get:

$$H_m = \frac{\pi}{3}\tau_0 LR^4 B_0^2. \quad (13)$$

Like in the cylindrical constant current non force-free case, we assume that N_{turns} is equal to 0.5 and 10.

References

- Aarnio, A.N., Matt, S.P., Stassun, K.G.: 2012, Mass Loss in Pre-main-sequence Stars via Coronal Mass Ejections and Implications for Angular Momentum Loss. *Astrophys. J.* **760**, 9. DOI. ADS.
- Airapetian, V.S., Gloer, A., Khazanov, G.V., Loyd, R.O.P., France, K., Sojka, J., Danchi, W.C., Liemohn, M.W.: 2017, How Hospitable Are Space Weather Affected Habitable Zones? The Role of Ion Escape. *Astrophys. J. Lett.* **836**, L3. DOI. ADS.
- Al-Haddad, N., Nieves-Chinchilla, T., Savani, N.P., Möstl, C., Marubashi, K., Hidalgo, M.A., Roussev, I.I., Poedts, S., Farrugia, C.J.: 2013, Magnetic Field Configuration Models and Reconstruction Methods for Interplanetary Coronal Mass Ejections. *Solar Phys.* **284**, 129. DOI. ADS.
- Andrews, M.D.: 2003, A Search for CMEs Associated with Big Flares. *Solar Phys.* **218**, 261. DOI. ADS.

- Anglada-Escudé, G., Amado, P.J., Barnes, J., Berdiñas, Z.M., Butler, R.P., Coleman, G.A.L., de La Cueva, I., Dreizler, S., Endl, M., Giesers, B., Jeffers, S.V., Jenkins, J.S., Jones, H.R.A., Kiraga, M., Kürster, M., López-González, M.J., Marvin, C.J., Morales, N., Morin, J., Nelson, R.P., Ortiz, J.L., Ofir, A., Paardekooper, S.-J., Reiners, A., Rodríguez, E., Rodríguez-López, C., Sarmiento, L.F., Strachan, J.P., Tsapras, Y., Tuomi, M., Zechmeister, M.: 2016, A terrestrial planet candidate in a temperate orbit around Proxima Centauri. *Nature* **536**, 437. DOI. ADS.
- Armstrong, D.J., Pugh, C.E., Broomhall, A.-M., Brown, D.J.A., Lund, M.N., Osborn, H.P., Pollacco, D.L.: 2016, The host stars of Kepler’s habitable exoplanets: superflares, rotation and activity. *Mon. Not. Roy. Astron. Soc.* **455**, 3110. DOI. ADS.
- Aulanier, G., Démoulin, P., Schrijver, C.J., Janvier, M., Pariat, E., Schmieder, B.: 2013, The standard flare model in three dimensions. II. Upper limit on solar flare energy. *Astron. Astrophys.* **549**, A66. DOI. ADS.
- Bastian, T.S., Pick, M., Kerdran, A., Maia, D., Vourlidas, A.: 2001, The Coronal Mass Ejection of 1998 April 20: Direct Imaging at Radio Wavelengths. *Astrophys. J. Lett.* **558**, L65. DOI. ADS.
- Berger, M.A.: 1984, Rigorous new limits on magnetic helicity dissipation in the solar corona. *Geophys. Astrophys. Fluid Dyn.* **30**, 79. DOI. ADS.
- Bosman, E., Bothmer, V., Nisticò, G., Vourlidas, A., Howard, R.A., Davies, J.A.: 2012, Three-Dimensional Properties of Coronal Mass Ejections from STEREO/SECCHI Observations. *Solar Phys.* **281**, 167. DOI. ADS.
- Bothmer, V., Schwenn, R.: 1998, The structure and origin of magnetic clouds in the solar wind. *Annales Geophysicae* **16**, 1. DOI. ADS.
- Chapman, S., Ferraro, V.C.A.: 1930, A New Theory of Magnetic Storms. *Nature* **126**, 129. DOI. ADS.
- Chintzoglou, G., Patsourakos, S., Vourlidas, A.: 2015, Formation of Magnetic Flux Ropes during a Confined Flaring Well before the Onset of a Pair of Major Coronal Mass Ejections. *Astrophys. J.* **809**, 34. DOI. ADS.
- Cid, C., Hidalgo, M.A., Nieves-Chinchilla, T., Sequeiros, J., Viñas, A.F.: 2002, Plasma and Magnetic Field Inside Magnetic Clouds: a Global Study. *Solar Phys.* **207**, 187. DOI. ADS.
- Cliver, E.W., Tylka, A.J., Dietrich, W.F., Ling, A.G.: 2014, On a Solar Origin for the Cosmicogenic Nuclide Event of 775 A.D. *Astrophys. J.* **781**, 32. DOI. ADS.
- Cunha, D., Correia, A.C.M., Laskar, J.: 2015, Spin evolution of Earth-sized exoplanets, including atmospheric tides and core-mantle friction. *International Journal of Astrobiology* **14**, 233. DOI. ADS.
- Dasso, S., Mandrini, C.H., Démoulin, P., Luoni, M.L.: 2006, A new model-independent method to compute magnetic helicity in magnetic clouds. *Astron. Astrophys.* **455**, 349. DOI. ADS.
- Davenport, J.R.A., Kipping, D.M., Sasselov, D., Matthews, J.M., Cameron, C.: 2016, MOST Observations of Our Nearest Neighbor: Flares on Proxima Centauri. *Astrophys. J. Lett.* **829**, L31. DOI. ADS.
- Démoulin, P., Dasso, S.: 2009, Causes and consequences of magnetic cloud expansion. *Astron. Astrophys.* **498**, 551. DOI. ADS.
- Démoulin, P., Janvier, M., Dasso, S.: 2016, Magnetic Flux and Helicity of Magnetic Clouds. *Solar Phys.* **291**, 531. DOI. ADS.
- Démoulin, P., Mandrini, C.H., van Driel-Gesztelyi, L., Thompson, B.J., Plunkett, S., Kovári, Z., Aulanier, G., Young, A.: 2002, What is the source of the magnetic helicity shed by CMEs? The long-term helicity budget of AR 7978. *Astron. Astrophys.* **382**, 650. DOI. ADS.
- DeVore, C.R.: 2000, Magnetic Helicity Generation by Solar Differential Rotation. *Astrophys. J.* **539**, 944. DOI. ADS.
- Donati, J.-F., Morin, J., Petit, P., Delfosse, X., Forveille, T., Aurière, M., Cabanac, R., Dintrans, B., Fares, R., Gastine, T., Jardine, M.M., Lignières, F., Paletou, F., Ramirez Velez, J.C., Théado, S.: 2008, Large-scale magnetic topologies of early M dwarfs. *Mon. Not. Roy. Astron. Soc.* **390**, 545. DOI. ADS.
- Dong, C., Lingam, M., Ma, Y., Cohen, O.: 2017, Is Proxima Centauri b habitable? – A study of atmospheric loss. *ArXiv e-prints*. ADS.
- Drake, J.J., Cohen, O., Yashiro, S., Gopalswamy, N.: 2013, Implications of Mass and Energy Loss due to Coronal Mass Ejections on Magnetically Active Stars. *Astrophys. J.* **764**, 170. DOI. ADS.
- Forbes, T.G.: 2000, A review on the genesis of coronal mass ejections. *J. Geophys. Res.* **105**, 23153. DOI. ADS.

- Forsyth, R.J., Bothmer, V., Cid, C., Crooker, N.U., Horbury, T.S., Kecskemeti, K., Klecker, B., Linker, J.A., Odstrcil, D., Reiner, M.J., Richardson, I.G., Rodriguez-Pacheco, J., Schmidt, J.M., Wimmer-Schweingruber, R.F.: 2006, ICMEs in the Inner Heliosphere: Origin, Evolution and Propagation Effects. Report of Working Group G. *Space Sci. Rev.* **123**, 383. DOI. ADS.
- Garraffo, C., Drake, J.J., Cohen, O.: 2016, The Space Weather of Proxima Centauri b. *Astrophys. J. Lett.* **833**, L4. DOI. ADS.
- Gary, G.A., Moore, R.L.: 2004, Eruption of a Multiple-Turn Helical Magnetic Flux Tube in a Large Flare: Evidence for External and Internal Reconnection That Fits the Breakout Model of Solar Magnetic Eruptions. *Astrophys. J.* **611**, 545. DOI. ADS.
- Georgoulis, M.K., Tziotziou, K., Raouafi, N.-E.: 2012, Magnetic Energy and Helicity Budgets in the Active-region Solar Corona. II. Nonlinear Force-free Approximation. *Astrophys. J.* **759**, 1. DOI. ADS.
- Georgoulis, M.K., Rust, D.M., Pevtsov, A.A., Bernasconi, P.N., Kuzanyan, K.M.: 2009, Solar Magnetic Helicity Injected into the Heliosphere: Magnitude, Balance, and Periodicities Over Solar Cycle 23. *Astrophys. J. Lett.* **705**, L48. DOI. ADS.
- Gibson, S.E., Fan, Y.: 2008, Partially ejected flux ropes: Implications for interplanetary coronal mass ejections. *J. Geophys. Res. Space Phys.* **113**, A09103. DOI. ADS.
- Gladman, B., Quinn, D.D., Nicholson, P., Rand, R.: 1996, Synchronous Locking of Tidally Evolving Satellites. *Icarus* **122**, 166. DOI. ADS.
- Gold, T., Hoyle, F.: 1960, On the origin of solar flares. *Mon. Not. Roy. Astron. Soc.* **120**, 89. DOI. ADS.
- Good, S.W., Forsyth, R.J., Raines, J.M., Gershman, D.J., Slavin, J.A., Zurbuchen, T.H.: 2015, Radial Evolution of a Magnetic Cloud: MESSENGER, STEREO, and Venus Express Observations. *Astrophys. J.* **807**, 177. DOI. ADS.
- Green, L.M., López fuentes, M.C., Mandrini, C.H., Démoulin, P., Van Driel-Gesztelyi, L., Culhane, J.L.: 2002, The Magnetic Helicity Budget of a cme-Prolific Active Region. *Solar Phys.* **208**, 43. DOI. ADS.
- Grißmeier, J.-M., Stadelmann, A., Penz, T., Lammer, H., Selsis, F., Ribas, I., Guinan, E.F., Mutschmann, U., Biernat, H.K., Weiss, W.W.: 2004, The effect of tidal locking on the magnetospheric and atmospheric evolution of “Hot Jupiters”. *Astron. Astrophys.* **425**, 753. DOI. ADS.
- Grißmeier, J.-M., Stadelmann, A., Mutschmann, U., Belisheva, N.K., Lammer, H., Biernat, H.K.: 2005, Cosmic Ray Impact on Extrasolar Earth-Like Planets in Close-in Habitable Zones. *Astrobiology* **5**, 587. DOI. ADS.
- Guo, Y., Ding, M.D., Cheng, X., Zhao, J., Pariat, E.: 2013, Twist Accumulation and Topology Structure of a Solar Magnetic Flux Rope. *Astrophys. J.* **779**, 157. DOI. ADS.
- Hariharan, K., Ramesh, R., Kathiravan, C., Wang, T.J.: 2016, Simultaneous Near-Sun Observations of a Moving Type IV Radio Burst and the Associated White-Light Coronal Mass Ejection. *Solar Phys.* **291**, 1405. DOI. ADS.
- Harra, L.K., Schrijver, C.J., Janvier, M., Toriumi, S., Hudson, H., Matthews, S., Woods, M.M., Hara, H., Guedel, M., Kowalski, A., Osten, R., Kusano, K., Lueftinger, T.: 2016, The Characteristics of Solar X-Class Flares and CMEs: A Paradigm for Stellar Superflares and Eruptions? *Solar Phys.* **291**, 1761. DOI. ADS.
- Hidalgo, M.A., Cid, C., Medina, J., Viñas, A.F.: 2000, A new model for the topology of magnetic clouds in the solar wind. *Solar Phys.* **194**, 165. DOI. ADS.
- Houdebine, E.R., Foing, B.H., Rodono, M.: 1990, Dynamics of flares on late-type dMe stars. I - Flare mass ejections and stellar evolution. *Astron. Astrophys.* **238**, 249. ADS.
- Howard, T.A., Stovall, K., Dowell, J., Taylor, G.B., White, S.M.: 2016, Measuring the Magnetic Field of Coronal Mass Ejections Near the Sun Using Pulsars. *Astrophys. J.* **831**, 208. DOI. ADS.
- Hu, Q., Qiu, J., Dasgupta, B., Khare, A., Webb, G.M.: 2014, Structures of Interplanetary Magnetic Flux Ropes and Comparison with Their Solar Sources. *Astrophys. J.* **793**, 53. DOI. ADS.
- Isavnin, A., Vourlidas, A., Kilpua, E.K.J.: 2014, Three-Dimensional Evolution of Flux-Rope CMEs and Its Relation to the Local Orientation of the Heliospheric Current Sheet. *Solar Phys.* **289**, 2141. DOI. ADS.
- Jakosky, B.M., Grebowsky, J.M., Luhmann, J.G., Connerney, J., Eparvier, F., Ergun, R., Halekas, J., Larson, D., Mahaffy, P., McFadden, J., Mitchell, D.F., Schneider, N., Zurek, R., Bougher, S., Brain, D., Ma, Y.J., Mazelle, C., Andersson, L., Andrews, D., Baird, D., Baker, D., Bell, J.M., Benna, M., Chaffin, M., Chamberlin, P., Chaufray, Y.-Y., Clarke,

- J., Collinson, G., Combi, M., Crary, F., Cravens, T., Crismani, M., Curry, S., Curtis, D., Deighan, J., Delory, G., Dewey, R., DiBraccio, G., Dong, C., Dong, Y., Dunn, P., Elrod, M., England, S., Eriksson, A., Espley, J., Evans, S., Fang, X., Fillingim, M., Fortier, K., Fowler, C.M., Fox, J., Gröller, H., Guzewich, S., Hara, T., Harada, Y., Holsclaw, G., Jain, S.K., Jolitz, R., Leblanc, F., Lee, C.O., Lee, Y., Lefevre, F., Lillis, R., Livi, R., Lo, D., Mayyasi, M., McClintock, W., McEnulty, T., Modolo, R., Montmessin, F., Morooka, M., Nagy, A., Olsen, K., Peterson, W., Rahmati, A., Ruhunusiri, S., Russell, C.T., Sakai, S., Sauvaud, J.-A., Seki, K., Steckiewicz, M., Stevens, M., Stewart, A.I.F., Stiepen, A., Stone, S., Tennishev, V., Thiemann, E., Tolson, R., Toubanc, D., Vogt, M., Weber, T., Withers, P., Woods, T., Yelle, R.: 2015, MAVEN observations of the response of Mars to an interplanetary coronal mass ejection. *Science* **350**, 0210. DOI. ADS.
- Jensen, E.A., Russell, C.T.: 2008, Faraday rotation observations of CMEs. *Geophys. Res. Lett.* **35**, L02103. DOI. ADS.
- Kane, S.R., Hill, M.L., Kasting, J.F., Kopparapu, R.K., Quintana, E.V., Barclay, T., Batalha, N.M., Borucki, W.J., Ciardi, D.R., Haghighipour, N., Hinkel, N.R., Kaltenegger, L., Selsis, F., Torres, G.: 2016, A Catalog of Kepler Habitable Zone Exoplanet Candidates. *Astrophys. J.* **830**, 1. DOI. ADS.
- Karoff, C., Knudsen, M.F., De Cat, P., Bonanno, A., Fogtman-Schulz, A., Fu, J., Frasca, A., Inceoglu, F., Olsen, J., Zhang, Y., Hou, Y., Wang, Y., Shi, J., Zhang, W.: 2016, Observational evidence for enhanced magnetic activity of superflare stars. *Nature Communications* **7**, 11058. DOI. ADS.
- Kasting, J.F., Whitmire, D.P., Reynolds, R.T.: 1993, Habitable Zones around Main Sequence Stars. *Icarus* **101**, 108. DOI. ADS.
- Kataoka, R., Ebisuzaki, T., Kusano, K., Shiota, D., Inoue, S., Yamamoto, T.T., Tokumaru, M.: 2009, Three-dimensional MHD modeling of the solar wind structures associated with 13 December 2006 coronal mass ejection. *J. Geophys. Res. Space Phys.* **114**, A10102. DOI. ADS.
- Kay, C., Opher, M., Evans, R.M.: 2013, Forecasting a Coronal Mass Ejection's Altered Trajectory: ForeCAT. *Astrophys. J.* **775**, 5. DOI. ADS.
- Kay, C., Opher, M., Kornbleuth, M.: 2016, Probability of CME Impact on Exoplanets Orbiting M Dwarfs and Solar-like Stars. *Astrophys. J.* **826**, 195. DOI. ADS.
- Kazachenko, M.D., Canfield, R.C., Longcope, D.W., Qiu, J., Des Jardins, A., Nightingale, R.W.: 2009, Sunspot Rotation, Flare Energetics, and Flux Rope Helicity: The Eruptive Flare on 2005 May 13. *Astrophys. J.* **704**, 1146. DOI. ADS.
- Khodachenko, M.L., Ribas, I., Lammer, H., Griefmeier, J.-M., Leitner, M., Selsis, F., Eiroa, C., Hanslmeier, A., Biernat, H.K., Farrugia, C.J., Rucker, H.O.: 2007, Coronal Mass Ejection (CME) Activity of Low Mass M Stars as An Important Factor for The Habitability of Terrestrial Exoplanets. I. CME Impact on Expected Magnetospheres of Earth-Like Exoplanets in Close-In Habitable Zones. *Astrobiology* **7**, 167. DOI. ADS.
- Kliem, B., Rust, S., Seehafer, N.: 2011, Helicity transport in a simulated coronal mass ejection. In: Bonanno, A., de Gouveia Dal Pino, E., Kosovichev, A.G. (eds.) *Advances in Plasma Astrophysics, IAU Symposium* **274**, 125. DOI. ADS.
- Kooi, J.E., Fischer, P.D., Buffo, J.J., Spangler, S.R.: 2016, VLA Measurements of Faraday Rotation through Coronal Mass Ejections. *ArXiv e-prints*. ADS.
- Kumar, A., Rust, D.M.: 1996, Interplanetary magnetic clouds, helicity conservation, and current-core flux-ropes. *J. Geophys. Res.* **101**, 15667. DOI. ADS.
- Kunkel, V., Chen, J.: 2010, Evolution of a Coronal Mass Ejection and its Magnetic Field in Interplanetary Space. *Astrophys. J. Lett.* **715**, L80. DOI. ADS.
- Lammer, H., Lichtenegger, H.I.M., Kulikov, Y.N., Griefmeier, J.-M., Terada, N., Erkaev, N.V., Biernat, H.K., Khodachenko, M.L., Ribas, I., Penz, T., Selsis, F.: 2007, Coronal Mass Ejection (CME) Activity of Low Mass M Stars as An Important Factor for The Habitability of Terrestrial Exoplanets. II. CME-Induced Ion Pick Up of Earth-like Exoplanets in Close-In Habitable Zones. *Astrobiology* **7**, 185. DOI. ADS.
- Leconte, J., Wu, H., Menou, K., Murray, N.: 2015, Asynchronous rotation of Earth-mass planets in the habitable zone of lower-mass stars. *Science* **347**, 632. DOI. ADS.
- Leitner, M., Farrugia, C.J., Möstl, C., Ogilvie, K.W., Galvin, A.B., Schwenn, R., Biernat, H.K.: 2007, Consequences of the force-free model of magnetic clouds for their heliospheric evolution. *J. Geophys. Res. Space Phys.* **112**, A06113. DOI. ADS.
- Leitzinger, M., Odert, P., Ribas, I., Hanslmeier, A., Lammer, H., Khodachenko, M.L., Zaqarashvili, T.V., Rucker, H.O.: 2011, Search for indications of stellar mass ejections using FUV spectra. *Astron. Astrophys.* **536**, A62. DOI. ADS.

- Leitzinger, M., Odert, P., Greimel, R., Korhonen, H., Guenther, E.W., Hanslmeier, A., Lammer, H., Khodachenko, M.L.: 2014, A search for flares and mass ejections on young late-type stars in the open cluster Blanco-1. *Mon. Not. Roy. Astron. Soc.* **443**, 898. DOI. ADS.
- Lepping, R.P., Berdichevsky, D.B., Wu, C.-C., Szabo, A., Narock, T., Mariani, F., Lazarus, A.J., Quivers, A.J.: 2006, A summary of WIND magnetic clouds for years 1995-2003: model-fitted parameters, associated errors and classifications. *Annales Geophysicae* **24**, 215. DOI. ADS.
- Liu, Y., Richardson, J.D., Belcher, J.W.: 2005, A statistical study of the properties of interplanetary coronal mass ejections from 0.3 to 5.4 AU. *Planet. Spa. Sci.* **53**, 3. DOI. ADS.
- Lundquist, S.: 1950, *Ark. Fys.* **2**(361).
- Luoni, M.L., Mandrini, C.H., Dasso, S., van Driel-Gesztelyi, L., Démoulin, P.: 2005, Tracing magnetic helicity from the solar corona to the interplanetary space. *Journal of Atmospheric and Solar-Terrestrial Physics* **67**, 1734. DOI. ADS.
- Lynch, B.J., Zurbuchen, T.H., Fisk, L.A., Antiochos, S.K.: 2003, Internal structure of magnetic clouds: Plasma and composition. *J. Geophys. Res. Space Phys.* **108**, 1239. DOI. ADS.
- Lynch, B.J., Gruesbeck, J.R., Zurbuchen, T.H., Antiochos, S.K.: 2005, Solar cycle-dependent helicity transport by magnetic clouds. *J. Geophys. Res. Space Phys.* **110**, A08107. DOI. ADS.
- Lynch, B.J., Antiochos, S.K., DeVore, C.R., Luhmann, J.G., Zurbuchen, T.H.: 2008, Topological Evolution of a Fast Magnetic Breakout CME in Three Dimensions. *Astrophys. J.* **683**, 1192. DOI. ADS.
- MacNeice, P., Antiochos, S.K., Phillips, A., Spicer, D.S., DeVore, C.R., Olson, K.: 2004, A Numerical Study of the Breakout Model for Coronal Mass Ejection Initiation. *Astrophys. J.* **614**, 1028. DOI. ADS.
- Maehara, H., Shibayama, T., Notsu, S., Notsu, Y., Nagao, T., Kusaba, S., Honda, S., Nogami, D., Shibata, K.: 2012, Superflares on solar-type stars. *Nature* **485**, 478. DOI. ADS.
- Mancuso, S., Garzelli, M.V.: 2013, Radial profile of the inner heliospheric magnetic field as deduced from Faraday rotation observations. *Astron. Astrophys.* **553**, A100. DOI. ADS.
- Mandrini, C.H., Pohjolainen, S., Dasso, S., Green, L.M., Démoulin, P., van Driel-Gesztelyi, L., Copperwheat, C., Foley, C.: 2005, Interplanetary flux rope ejected from an X-ray bright point. The smallest magnetic cloud source-region ever observed. *Astron. Astrophys.* **434**, 725. DOI. ADS.
- Moraitis, K., Tziotziou, K., Georgoulis, M.K., Archontis, V.: 2014, Validation and Benchmarking of a Practical Free Magnetic Energy and Relative Magnetic Helicity Budget Calculation in Solar Magnetic Structures. *Solar Phys.* **289**, 4453. DOI. ADS.
- Möstl, C., Farrugia, C.J., Kilpua, E.K.J., Jian, L.K., Liu, Y., Eastwood, J.P., Harrison, R.A., Webb, D.F., Temmer, M., Odstrcil, D., Davies, J.A., Rollett, T., Luhmann, J.G., Nitta, N., Mulligan, T., Jensen, E.A., Forsyth, R., Lavraud, B., de Koning, C.A., Veronig, A.M., Galvin, A.B., Zhang, T.L., Anderson, B.J.: 2012, Multi-point Shock and Flux Rope Analysis of Multiple Interplanetary Coronal Mass Ejections around 2010 August 1 in the Inner Heliosphere. *Astrophys. J.* **758**, 10. DOI. ADS.
- Nakwacki, M.S., Dasso, S., Démoulin, P., Mandrini, C.H., Gulisano, A.M.: 2011, Dynamical evolution of a magnetic cloud from the Sun to 5.4 AU. *Astron. Astrophys.* **535**, A52. DOI. ADS.
- Nieves-Chinchilla, T., Linton, M.G., Hidalgo, M.A., Vourlidas, A., Savani, N.P., Szabo, A., Farrugia, C., Yu, W.: 2016, A Circular-cylindrical Flux-rope Analytical Model for Magnetic Clouds. *Astrophys. J.* **823**, 27. DOI. ADS.
- Nindos, A., Andrews, M.D.: 2004, The Association of Big Flares and Coronal Mass Ejections: What Is the Role of Magnetic Helicity? *Astrophys. J. Lett.* **616**, L175. DOI. ADS.
- Nindos, A., Zhang, J., Zhang, H.: 2003, The Magnetic Helicity Budget of Solar Active Regions and Coronal Mass Ejections. *Astrophys. J.* **594**, 1033. DOI. ADS.
- Nindos, A., Patsourakos, S., Vourlidas, A., Tagikakos, C.: 2015, How Common Are Hot Magnetic Flux Ropes in the Low Solar Corona? A Statistical Study of EUV Observations. *Astrophys. J.* **808**, 117. DOI. ADS.
- Nogami, D., Notsu, Y., Honda, S., Maehara, H., Notsu, S., Shibayama, T., Shibata, K.: 2014, Two sun-like superflare stars rotating as slow as the Sun*. *Pub. Astron. Soc. Japan* **66**, L4. DOI. ADS.
- Osten, R.A., Wolk, S.J.: 2015, Connecting Flares and Transient Mass-loss Events in Magnetically Active Stars. *Astrophys. J.* **809**, 79. DOI. ADS.

- Osten, R., Livio, M., Lubow, S., Pringle, J.E., Soderblom, D., Valenti, J.: 2013, Coronal Mass Ejections as a Mechanism for Producing IR Variability in Debris Disks. *Astrophys. J. Lett.* **765**, L44. DOI. ADS.
- Pariat, E., Nindos, A., Démoulin, P., Berger, M.A.: 2006, What is the spatial distribution of magnetic helicity injected in a solar active region? *Astron. Astrophys.* **452**, 623. DOI. ADS.
- Patsourakos, S., Georgoulis, M.K.: 2016, Near-Sun and 1 AU magnetic field of coronal mass ejections: a parametric study. *Astron. Astrophys.* **595**, A121. DOI. ADS.
- Patsourakos, S., Georgoulis, M.K., Vourlidas, A., Nindos, A., Sarris, T., Anagnostopoulos, G., Anastasiadis, A., Chintzoglou, G., Daglis, I.A., Gontikakis, C., Hatzigeorgiu, N., Iliopoulos, A.C., Katsavrias, C., Kouloumvakos, A., Moraitis, K., Nieves-Chinchilla, T., Pavlos, G., Sarafopoulos, D., Syntelis, P., Tsironis, C., Tziotziou, K., Vogiatzis, I.I., Balasis, G., Georgiou, M., Karakatsanis, L.P., Malandraki, O.E., Papadimitriou, C., Odstrčil, D., Pavlos, E.G., Podlachikova, O., Sandberg, I., Turner, D.L., Xenakis, M.N., Sarris, E., Tsinganos, K., Vlahos, L.: 2016, The Major Geoeffective Solar Eruptions of 2012 March 7: Comprehensive Sun-to-Earth Analysis. *Astrophys. J.* **817**, 14. DOI. ADS.
- Patzold, M., Bird, M.K., Volland, H., Levy, G.S., Seidel, B.L., Stelzried, C.T.: 1987, The mean coronal magnetic field determined from HELIOS Faraday rotation measurements. *Solar Phys.* **109**, 91. DOI. ADS.
- Poomvisee, W., Gopalswamy, N., Yashiro, S., Kwon, R.-Y., Olmedo, O.: 2012, Determination of the Heliospheric Radial Magnetic Field from the Standoff Distance of a CME-driven Shock Observed by the STEREO Spacecraft. *Astrophys. J.* **758**, 118. DOI. ADS.
- Priest, E.R., Longcope, D.W., Janvier, M.: 2016, Evolution of Magnetic Helicity During Eruptive Flares and Coronal Mass Ejections. *Solar Phys.* **291**, 2017. DOI. ADS.
- Régnier, S., Canfield, R.C.: 2006, Evolution of magnetic fields and energetics of flares in active region 8210. *Astron. Astrophys.* **451**, 319. DOI. ADS.
- Riley, P., Linker, J.A., Lionello, R., Mikić, Z., Odstrčil, D., Hidalgo, M.A., Cid, C., Hu, Q., Lepping, R.P., Lynch, B.J., Rees, A.: 2004, Fitting flux ropes to a global MHD solution: a comparison of techniques. *Journal of Atmospheric and Solar-Terrestrial Physics* **66**, 1321. DOI. ADS.
- Savani, N.P., Vourlidas, A., Szabo, A., Mays, M.L., Richardson, I.G., Thompson, B.J., Pulkkinen, A., Evans, R., Nieves-Chinchilla, T.: 2015, Predicting the magnetic vectors within coronal mass ejections arriving at Earth: 1. Initial architecture. *Space Weather* **13**, 374. DOI. ADS.
- Scalo, J., Kaltenecker, L., Segura, A.G., Fridlund, M., Ribas, I., Kulikov, Y.N., Grenfell, J.L., Rauer, H., Odert, P., Leitzinger, M., Selsis, F., Khodachenko, M.L., Eiroa, C., Kasting, J., Lammer, H.: 2007, M Stars as Targets for Terrestrial Exoplanet Searches And Biosignature Detection. *Astrobiology* **7**, 85. DOI. ADS.
- Schrijver, C.J., Beer, J., Baltensperger, U., Cliver, E.W., Güdel, M., Hudson, H.S., McCracken, K.G., Osten, R.A., Peter, T., Soderblom, D.R., Usoskin, I.G., Wolff, E.W.: 2012, Estimating the frequency of extremely energetic solar events, based on solar, stellar, lunar, and terrestrial records. *J. Geophys. Res. Space Phys.* **117**, A08103. DOI. ADS.
- See, V., Jardine, M., Vidotto, A.A., Petit, P., Marsden, S.C., Jeffers, S.V., do Nascimento, J.D.: 2014, The effects of stellar winds on the magnetospheres and potential habitability of exoplanets. *Astron. Astrophys.* **570**, A99. DOI. ADS.
- Selsis, F., Kasting, J.F., Levrard, B., Paillet, J., Ribas, I., Delfosse, X.: 2007, Habitable planets around the star Gliese 581? *Astron. Astrophys.* **476**, 1373. DOI. ADS.
- Semel, M.: 1989, Zeeman-Doppler imaging of active stars. I - Basic principles. *Astron. Astrophys.* **225**, 456. ADS.
- Shibata, K., Isobe, H., Hillier, A., Choudhuri, A.R., Maehara, H., Ishii, T.T., Shibayama, T., Notsu, S., Notsu, Y., Nagao, T., Honda, S., Nogami, D.: 2013, Can Superflares Occur on Our Sun? *Pub. Astron. Soc. Japan* **65**, 49. DOI. ADS.
- Shibayama, T., Maehara, H., Notsu, S., Notsu, Y., Nagao, T., Honda, S., Ishii, T.T., Nogami, D., Shibata, K.: 2013, Superflares on Solar-type Stars Observed with Kepler. I. Statistical Properties of Superflares. *Astrophys. J. Supp.* **209**, 5. DOI. ADS.
- Sun, X., Hoeksema, J.T., Liu, Y., Wiegmann, T., Hayashi, K., Chen, Q., Thalmann, J.: 2012, Evolution of Magnetic Field and Energy in a Major Eruptive Active Region Based on SDO/HMI Observation. *Astrophys. J.* **748**, 77. DOI. ADS.
- Thernisien, A., Vourlidas, A., Howard, R.A.: 2009, Forward Modeling of Coronal Mass Ejections Using STEREO/SECCHI Data. *Solar Phys.* **256**, 111. DOI. ADS.

- Toriumi, S., Schrijver, C.J., Harra, L.K., Hudson, H., Nagashima, K.: 2017, Magnetic Properties of Solar Active Regions That Govern Large Solar Flares and Eruptions. *Astrophys. J.* **834**, 56. DOI. ADS.
- Torres, G., Kipping, D.M., Fressin, F., Caldwell, D.A., Twicken, J.D., Ballard, S., Batalha, N.M., Bryson, S.T., Ciardi, D.R., Henze, C.E., Howell, S.B., Isaacson, H.T., Jenkins, J.M., Muirhead, P.S., Newton, E.R., Petigura, E.A., Barclay, T., Borucki, W.J., Crepp, J.R., Everett, M.E., Horch, E.P., Howard, A.W., Kolbl, R., Marcy, G.W., McCauliff, S., Quintana, E.V.: 2015, Validation of 12 Small Kepler Transiting Planets in the Habitable Zone. *Astrophys. J.* **800**, 99. DOI. ADS.
- Tun, S.D., Vourlidas, A.: 2013, Derivation of the Magnetic Field in a Coronal Mass Ejection Core via Multi-frequency Radio Imaging. *Astrophys. J.* **766**, 130. DOI. ADS.
- Tziotziou, K., Georgoulis, M.K., Liu, Y.: 2013, Interpreting Eruptive Behavior in NOAA AR 11158 via the Region's Magnetic Energy and Relative-helicity Budgets. *Astrophys. J.* **772**, 115. DOI. ADS.
- Tziotziou, K., Georgoulis, M.K., Raouafi, N.-E.: 2012, The Magnetic Energy-Helicity Diagram of Solar Active Regions. *Astrophys. J. Lett.* **759**, L4. DOI. ADS.
- Usoskin, I.G., Kromer, B., Ludlow, F., Beer, J., Friedrich, M., Kovaltsov, G.A., Solanki, S.K., Wacker, L.: 2013, The AD775 cosmic event revisited: the Sun is to blame. *Astron. Astrophys.* **552**, L3. DOI. ADS.
- Valori, G., Démoulin, P., Pariat, E.: 2012, Comparing Values of the Relative Magnetic Helicity in Finite Volumes. *Solar Phys.* **278**, 347. DOI. ADS.
- Vandas, M., Romashets, E.: 2016, Toroidal linear force-free magnetic fields with axial symmetry. *Astron. Astrophys.* **585**, A108. DOI. ADS.
- Vidotto, A.A., Jardine, M., Morin, J., Donati, J.-F., Lang, P., Russell, A.J.B.: 2013, Effects of M dwarf magnetic fields on potentially habitable planets. *Astron. Astrophys.* **557**, A67. DOI. ADS.
- Vidotto, A.A., Gregory, S.G., Jardine, M., Donati, J.F., Petit, P., Morin, J., Folsom, C.P., Bouvier, J., Cameron, A.C., Hussain, G., Marsden, S., Waite, I.A., Fares, R., Jeffers, S., do Nascimento, J.D.: 2014, Stellar magnetism: empirical trends with age and rotation. *Mon. Not. Roy. Astron. Soc.* **441**, 2361. DOI. ADS.
- Vourlidas, A., Subramanian, P., Dere, K.P., Howard, R.A.: 2000, Large-Angle Spectrometric Coronagraph Measurements of the Energetics of Coronal Mass Ejections. *Astrophys. J.* **534**, 456. DOI. ADS.
- Vrsnak, B., Ruzdjak, V., Rompolt, B., Rosa, D., Zlobec, P.: 1993, Kinematics and evolution of twist in the eruptive prominence of August 18, 1980. *Solar Phys.* **146**, 147. DOI. ADS.
- Vršnak, B., Magdalenic, J., Zlobec, P.: 2004, Band-splitting of coronal and interplanetary type II bursts. III. Physical conditions in the upper corona and interplanetary space. *Astron. Astrophys.* **413**, 753. DOI. ADS.
- Wang, Y., Zhuang, B., Hu, Q., Liu, R., Shen, C., Chi, Y.: 2016, On the twists of interplanetary magnetic flux ropes observed at 1 AU. *J. Geophys. Res. Space Phys.* **121**, 9316. DOI. ADS.
- Winslow, R.M., Lugaz, N., Philpott, L.C., Schwadron, N.A., Farrugia, C.J., Anderson, B.J., Smith, C.W.: 2015, Interplanetary coronal mass ejections from MESSENGER orbital observations at Mercury. *J. Geophys. Res. Space Phys.* **120**, 6101. DOI. ADS.
- Wood, B.E., Howard, R.A., Socker, D.G.: 2010, Reconstructing the Morphology of an Evolving Coronal Mass Ejection. *Astrophys. J.* **715**, 1524. DOI. ADS.
- Wu, C.-C., Lepping, R.P.: 2005, Relationships for predicting magnetic cloud-related geomagnetic storm intensity. *Journal of Atmospheric and Solar-Terrestrial Physics* **67**, 283. DOI. ADS.
- Yashiro, S., Gopalswamy, N., Akiyama, S., Michalek, G., Howard, R.A.: 2005, Visibility of coronal mass ejections as a function of flare location and intensity. *J. Geophys. Res. Space Phys.* **110**, A12S05. DOI. ADS.
- Zuluaga, J.I., Bustamante, S.: 2016, Geomagnetic properties of Proxima Centauri b analogues. *ArXiv e-prints, Submitted to ApJL*. ADS.

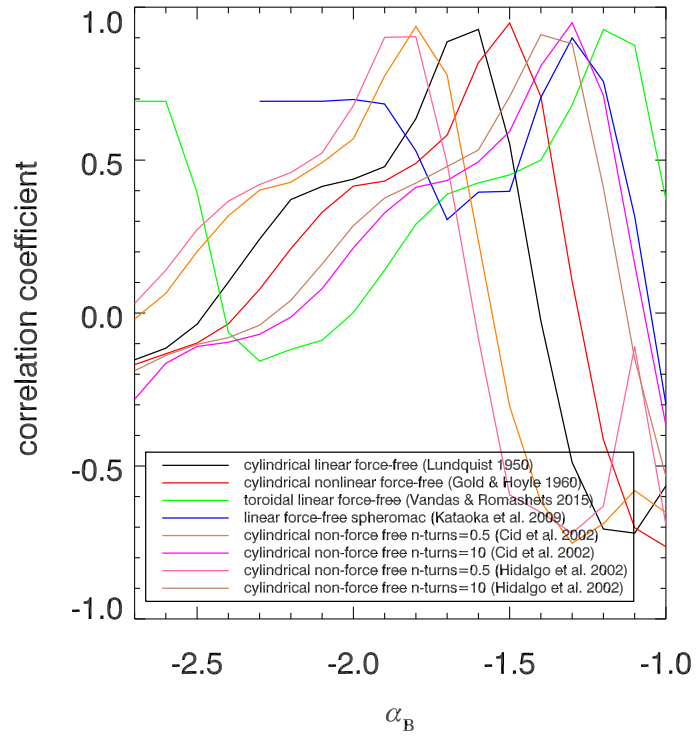


Figure 1. Correlation coefficient of the PDFs for the predicted $B_{1\text{AU}}$ and observed B_{MC} values at L1 as a function of α_B for the various employed models.

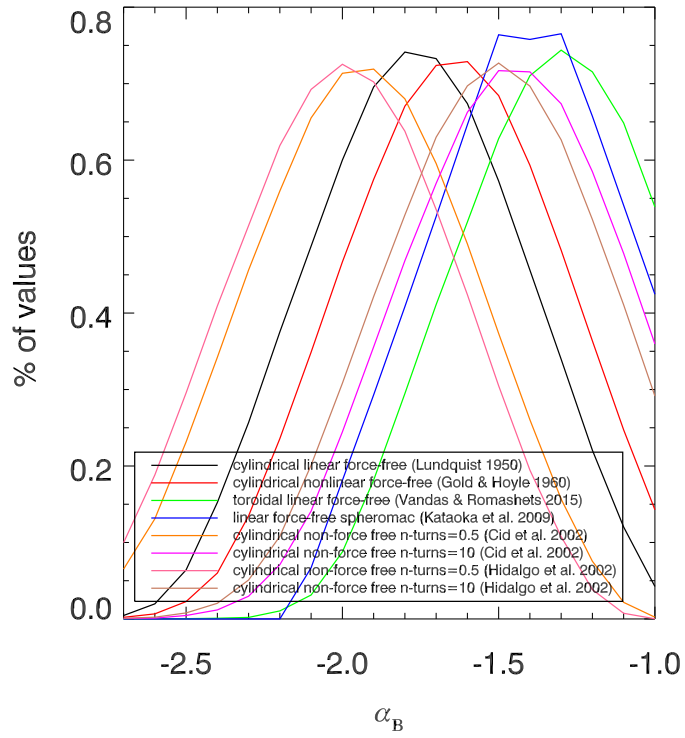


Figure 2. Fraction of $B_{1 \text{ AU}}$ values falling within the observed B_{MC} range of 4–45 nT as a function of α_B for the various employed models.

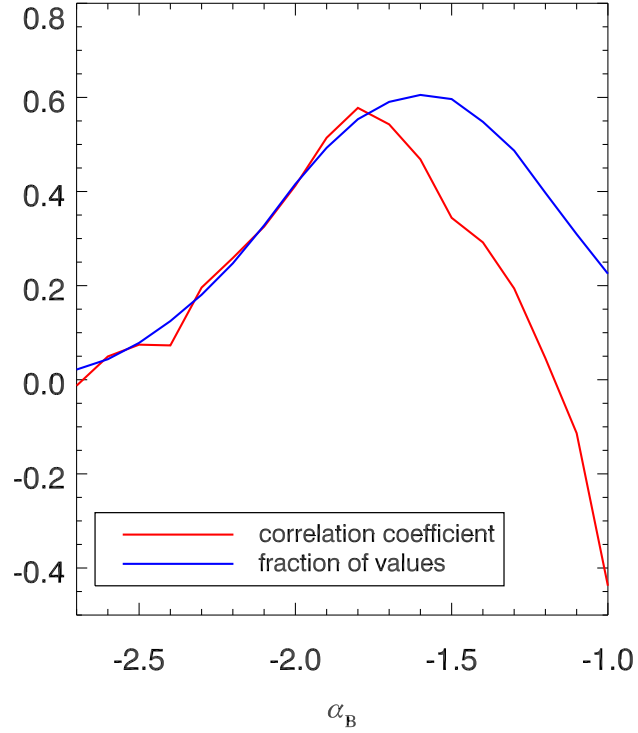


Figure 3. Model-averaged correlation coefficient of the PDF for the predicted $B_{1\text{AU}}$ and observed B_{MC} values at L1 as a function of α_B (red curve). Also shown is the respective fraction of $B_{1\text{AU}}$ values (blue curve) falling within the observed B_{MC} range. Both curves correspond to the respective averages of the various employed models as displayed in Figures 1 and 2.

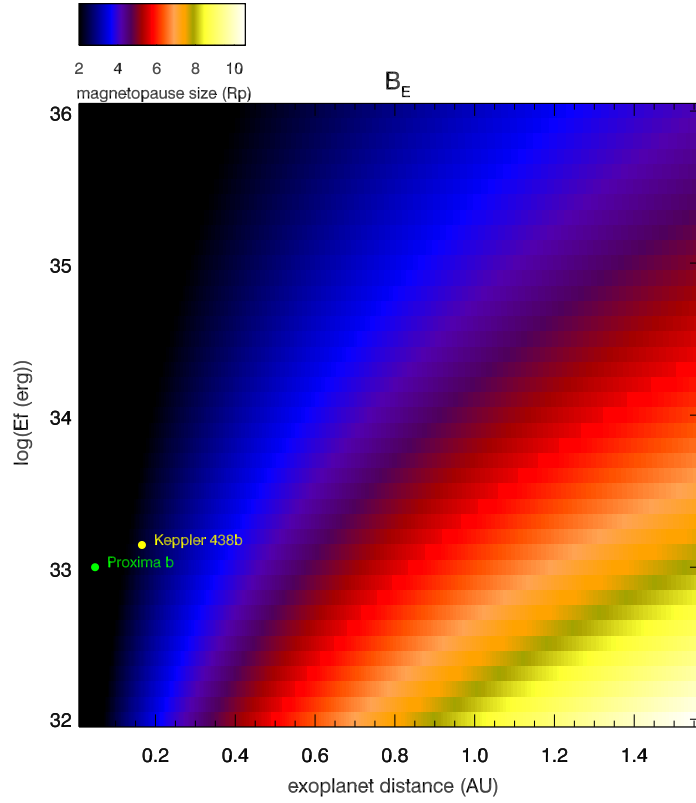


Figure 4. Exoplanet magnetopause radius (in units of planet radius) required to counterbalance the magnetic pressure of a CME arriving at its vicinity as a function of the exoplanet distance to, and the associated flare energy of, the planet’s mother star. Magnetopause sizes smaller than 2, representing a lower limit of magnetospheric size to avoid atmospheric erosion, are saturated with black. The index α_B is assumed equal to be -1.6 and the Lundquist model is used. The yellow and green circles correspond to two case-studies of exoplanets Kepler 438b and Proxima b, orbiting stars exhibiting superflares. It is assumed that the exoplanets have an equatorial magnetic field equal to the terrestrial one, $B_E \approx 0.333$ G.

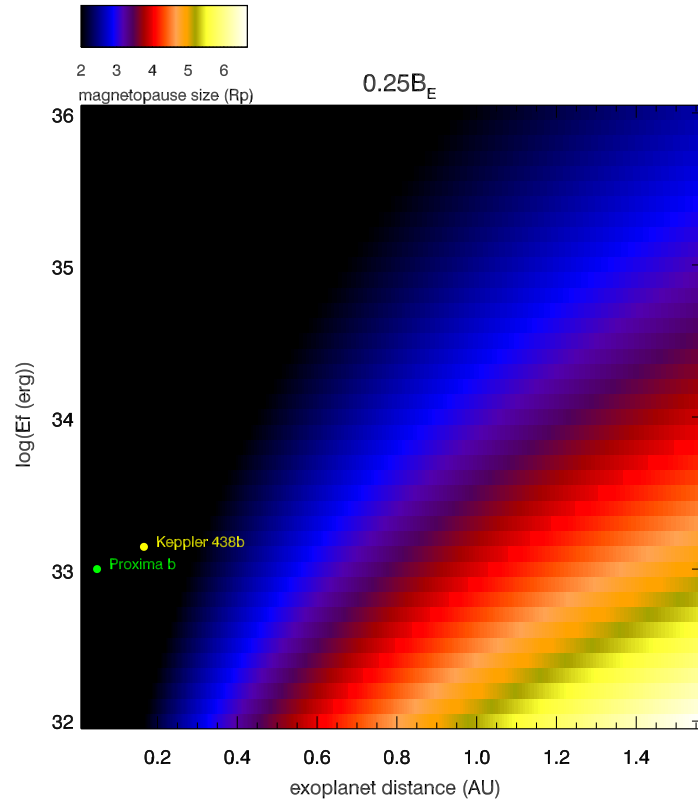


Figure 5. Same as Figure 4, but for an exoplanet equatorial magnetic field of ≈ 0.083 G, which is $\approx 25\%$ of the terrestrial value.

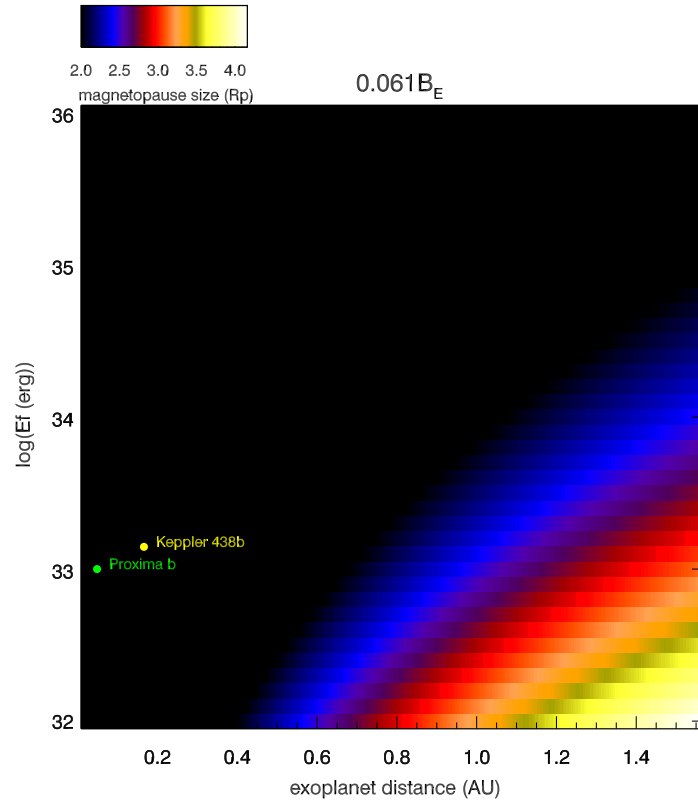


Figure 6. Same as Figure 4, but for an exoplanet equatorial magnetic field of ≈ 0.020 G, $\approx 6.1\%$ of the terrestrial value.

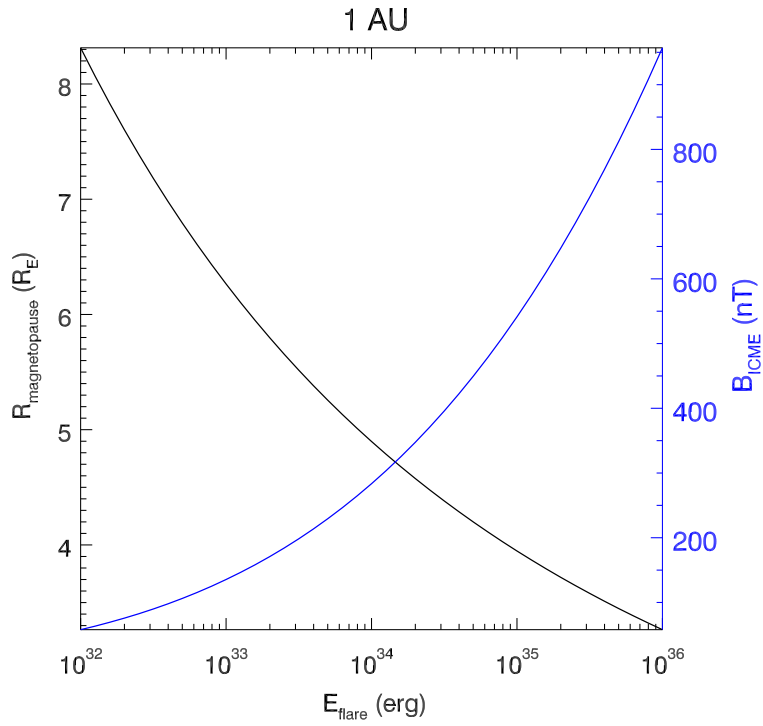


Figure 7. Terrestrial magnetopause radius size (black) and ICME magnetic field magnitude at 1 AU (blue) as a function of flare energy. The index α_B is equal to -1.6 and the Lundquist model is used.

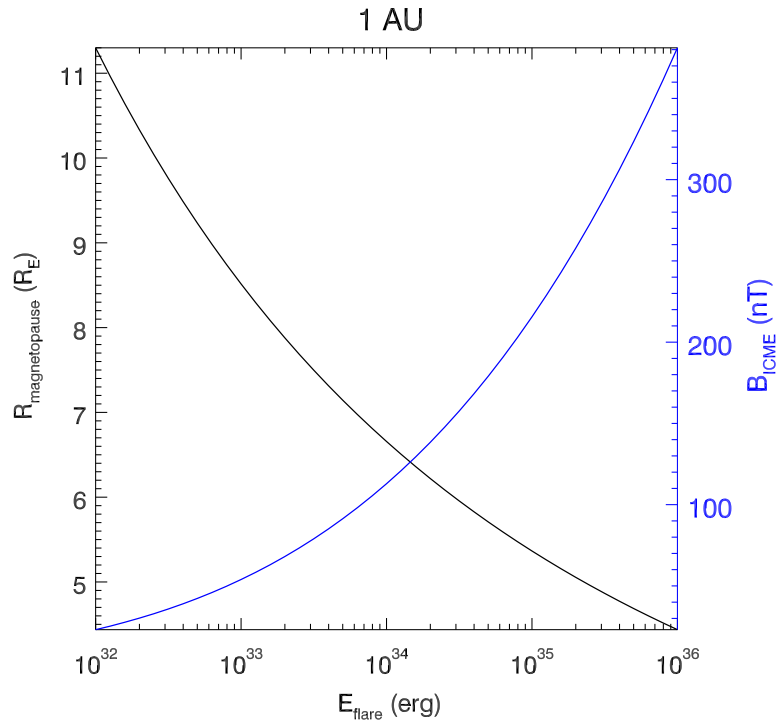


Figure 8. Terrestrial magnetopause radius size (black) and ICME magnetic field magnitude at 1 AU (blue) as a function of flare energy. The index α_B is equal to -1.9 and the Lundquist model is used.

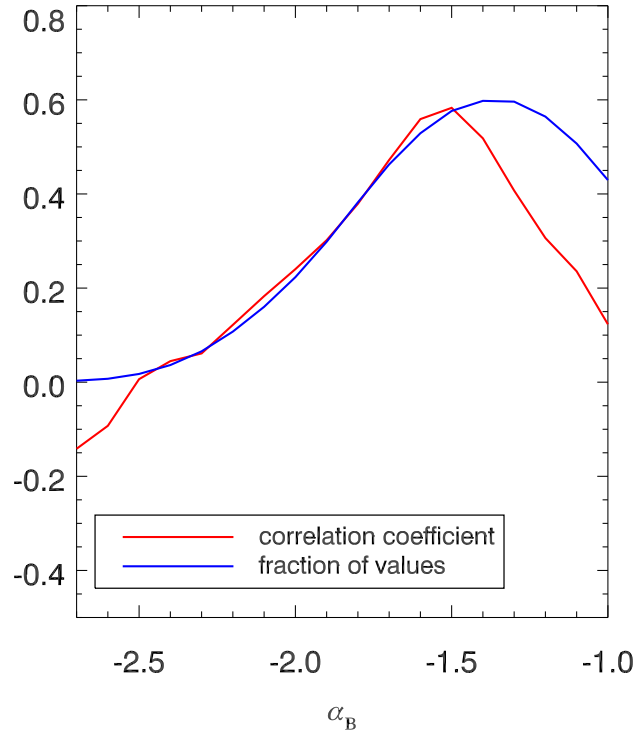


Figure 9. Model-averaged correlation coefficient of the PDF for the predicted $B_{1\text{AU}}$ and observed B_{MC} values at L1 as a function of α_B (red curve). Also shown is the respective fraction of $B_{1\text{AU}}$ values (blue curve) falling within the observed B_{MC} range. Calculations shown here are the same as in Figure 3 but use a randomly selected CME H_m value in the range 10 – 40% of the AR H_m value (a fixed 100% of the AR H_m is used in Figure 3).